A Variational Framework for Phase-Field Fracture Modeling with Applications to Fragmentation, Desiccation, Ductile Failure, and Spallation

Dissertation Defense

Tianchen (Gary) Hu

Department of Mechanical Engineering & Materials Science
Pratt School of Engineering
Duke University

Committee: John Dolbow
Wilkins Aquino
Johann Guilleminot
Manolis Viveakis
Benjamin Spencer

July 15th, 2021

Overview

Introduction
- Background
- Phase-field approach to fracture

The Variational Framework
- Thermodynamics
- The variational statement

Numerical Examples and Applications
- Towards Ductile Fracture
- Intergranular Fracture in Polycrystalline Materials
- Soil Desiccation

Conclusions and Future Work

Acknowledgements

References

Introduction
- Background
- Phase-field approach to fracture

The Variational Framework
- Thermodynamics
- The variational statement

Numerical Examples and Applications
- Towards Ductile Fracture
- Intergranular Fracture in Polycrystalline Materials
- Soil Desiccation

Conclusions and Future Work

Acknowledgements

References

- Fracture is a common phenomenon in engineering applications.

- Fracture is a common phenomenon in engineering applications.
- To characterize fracture by its **consequence**: fragmentation, desiccation, ductile failure, spallation, etc..

- Fracture is a common phenomenon in engineering applications.
- To characterize fracture by its **consequence**: fragmentation, desiccation, ductile failure, spallation, etc..

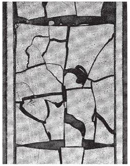

- Fracture is a common phenomenon in engineering applications.
- To characterize fracture by its **consequence**: fragmentation, desiccation, ductile failure, spallation, etc..

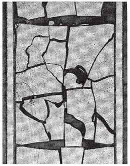


- Fracture is a common phenomenon in engineering applications.
- To characterize fracture by its **consequence**: fragmentation, desiccation, ductile failure, spallation, etc..

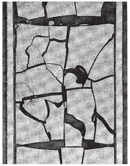

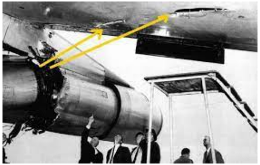

- Fracture is a common phenomenon in engineering applications.
- To characterize fracture by its **consequence**: fragmentation, desiccation, ductile failure, spallation, etc..

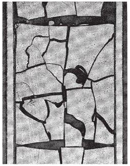

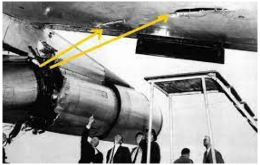


- Fracture is a common phenomenon in engineering applications.
- To characterize fracture by its **consequence**: fragmentation, desiccation, ductile failure, spallation, etc..
- To characterize fracture by its **development lifecycle**: defects, nucleation, propagation, branching, merging.

- Fracture is a common phenomenon in engineering applications.
- To characterize fracture by its **consequence**: fragmentation, desiccation, ductile failure, spallation, etc..
- To characterize fracture by its **development lifecycle**: defects, nucleation, propagation, branching, merging.

- Fracture is a common phenomenon in engineering applications.
- To characterize fracture by its **consequence**: fragmentation, desiccation, ductile failure, spallation, etc..
- To characterize fracture by its **development lifecycle**: defects, nucleation, propagation, branching, merging.

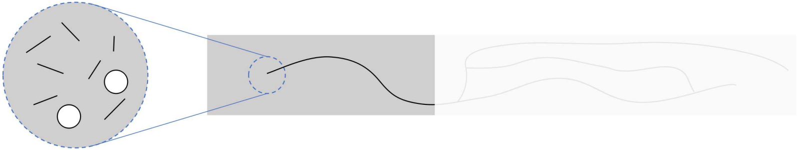

- Fracture is a common phenomenon in engineering applications.
- To characterize fracture by its **consequence**: fragmentation, desiccation, ductile failure, spallation, etc..
- To characterize fracture by its **development lifecycle**: defects, nucleation, propagation, branching, merging.

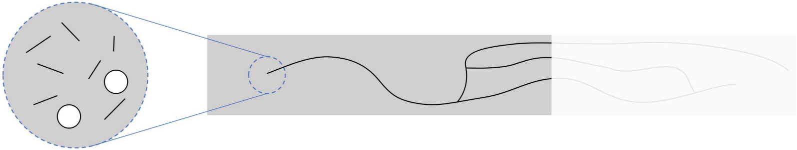

- Fracture is a common phenomenon in engineering applications.
- To characterize fracture by its **consequence**: fragmentation, desiccation, ductile failure, spallation, etc..
- To characterize fracture by its **development lifecycle**: defects, nucleation, propagation, branching, merging.

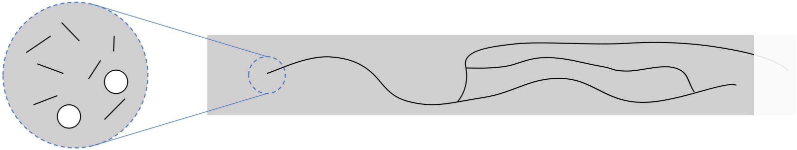

- Fracture is a common phenomenon in engineering applications.
- To characterize fracture by its **consequence**: fragmentation, desiccation, ductile failure, spallation, etc..
- To characterize fracture by its **development lifecycle**: defects, nucleation, propagation, branching, merging.
- To categorize fracture by **material response**:

- Fracture is a common phenomenon in engineering applications.
- To characterize fracture by its **consequence**: fragmentation, desiccation, ductile failure, spallation, etc..
- To characterize fracture by its **development lifecycle**: defects, nucleation, propagation, branching, merging.
- To categorize fracture by **material response**:
  - brittle fracture: singularities, abrupt failure, tiny fracture process zone;

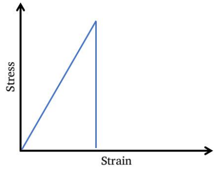

- Fracture is a common phenomenon in engineering applications.
- To characterize fracture by its **consequence**: fragmentation, desiccation, ductile failure, spallation, etc..
- To characterize fracture by its **development lifecycle**: defects, nucleation, propagation, branching, merging.
- To categorize fracture by **material response**:
  - brittle fracture: singularities, abrupt failure, tiny fracture process zone;
  - quasi-brittle fracture: softening, small fracture process zone;

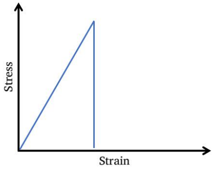

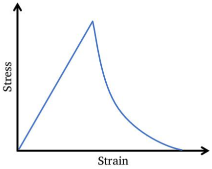

- Fracture is a common phenomenon in engineering applications.
- To characterize fracture by its **consequence**: fragmentation, desiccation, ductile failure, spallation, etc..
- To characterize fracture by its **development lifecycle**: defects, nucleation, propagation, branching, merging.
- To categorize fracture by **material response**:
  - brittle fracture: singularities, abrupt failure, tiny fracture process zone;
  - quasi-brittle fracture: softening, small fracture process zone;
  - cohesive fracture: softening, large fracture process zone;

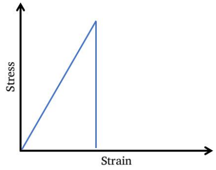

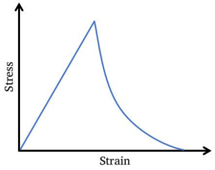

- Fracture is a common phenomenon in engineering applications.
- To characterize fracture by its **consequence**: fragmentation, desiccation, ductile failure, spallation, etc..
- To characterize fracture by its **development lifecycle**: defects, nucleation, propagation, branching, merging.
- To categorize fracture by **material response**:
  - brittle fracture: singularities, abrupt failure, tiny fracture process zone;
  - quasi-brittle fracture: softening, small fracture process zone;
  - cohesive fracture: softening, large fracture process zone;
  - ductile fracture: plastic deformation prior to fracture;
  - ...

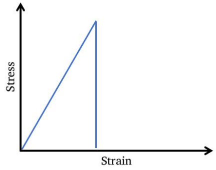

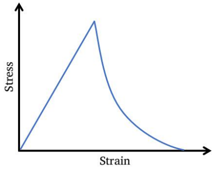

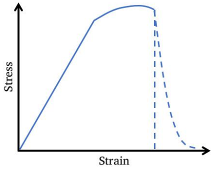

- Fracture is a common phenomenon in engineering applications.
- To characterize fracture by its **consequence**: fragmentation, desiccation, ductile failure, spallation, etc..
- To characterize fracture by its **development lifecycle**: defects, nucleation, propagation, branching, merging.
- To categorize fracture by **material response**:
  - brittle fracture: singularities, abrupt failure, tiny fracture process zone;
  - quasi-brittle fracture: softening, small fracture process zone;
  - cohesive fracture: softening, large fracture process zone;
  - ductile fracture: plastic deformation prior to fracture;
  - ...
- Coupling with other phenomena: dynamics, viscous dissipation, thermal effects, plasticity, creep, etc..

- Fracture is a common phenomenon in engineering applications.
- To characterize fracture by its **consequence**: fragmentation, desiccation, ductile failure, spallation, etc..
- To characterize fracture by its **development lifecycle**: defects, nucleation, propagation, branching, merging.
- To categorize fracture by **material response**:
  - brittle fracture: singularities, abrupt failure, tiny fracture process zone;
  - quasi-brittle fracture: softening, small fracture process zone;
  - cohesive fracture: softening, large fracture process zone;
  - ductile fracture: plastic deformation prior to fracture;
  - ...
- Coupling with other phenomena: dynamics, viscous dissipation, thermal effects, plasticity, creep, etc..

To date, fracture is still one of the most challenging phenomena to model and predict.

The permanent crack set Γ and its associated fracture energy

$$\Psi^f = \int_\Gamma \mathcal{G}_c \, \mathrm{d}A$$

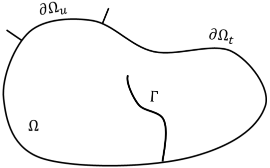

The permanent crack set Γ and its associated fracture energy

$$\Psi^f = \int_\Gamma \mathcal{G}_c \, \mathrm{d}A$$

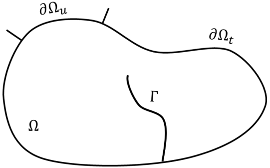

is approximated with

the crack surface density function $\gamma = \widehat{\gamma}_l(d)$:

$$\Psi^f \approx \int_\Omega \mathcal{G}_c \gamma \, \mathrm{d}V, \quad \gamma = \frac{1}{c_0 l}\left(\alpha + l^2 \boldsymbol{\nabla} d \cdot \boldsymbol{\nabla} d\right).$$

- $d \in [0, 1]$ is the phase field;
- $\alpha = \widehat{\alpha}(d)$ is the crack geometric function, $\widehat{\alpha}(0) = 0$, $\widehat{\alpha}(1) = 1$;
- $g = \widehat{g}(d)$ is the degradation function, $\widehat{g}(0) = 1$, $\widehat{g}(1) = 0$;
- c_0 is chosen such that

$$\lim_{l \to 0^+} \int_\Omega \mathcal{G}_c \gamma \, \mathrm{d}V = \int_\Gamma \mathcal{G}_c \, \mathrm{d}A.$$

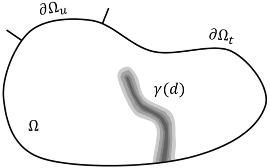

See [1] for more details.

Introduction
- Background
- Phase-field approach to fracture

The Variational Framework
- Thermodynamics
- The variational statement

Numerical Examples and Applications
- Towards Ductile Fracture
- Intergranular Fracture in Polycrystalline Materials
- Soil Desiccation

Conclusions and Future Work

Acknowledgements

References

- Working with the Helmholtz free energy density ψ, variables we are concerned with are

$$\boldsymbol{\phi}, \quad \boldsymbol{F}^p, \quad \bar{\varepsilon}^p, \quad d, \quad T.$$

- Conservations and thermodynamic laws:

$$\begin{aligned}
&\dot{\rho}_0 = 0,\\
&\rho_0 \mathbf{a} = \boldsymbol{\nabla}\cdot\boldsymbol{P} + \rho_0 \mathbf{b},\\
&\boldsymbol{P}\boldsymbol{F} = \boldsymbol{F}\boldsymbol{P}^T,\\
&f - \boldsymbol{\nabla}\cdot\boldsymbol{\xi} = 0,\\
&\dot{u} + \dot{k} = \mathcal{P}^{\text{ext}} + \rho_0 q - \boldsymbol{\nabla}\cdot\mathbf{h},\\
&\dot{s}^{\text{int}} = \dot{s} - \frac{\rho_0 q}{T} + \boldsymbol{\nabla}\cdot\frac{\mathbf{h}}{T} \geqslant 0.
\end{aligned}$$

- Working with the Helmholtz free energy density ψ, variables we are concerned with are

$$\boldsymbol{\phi}, \quad \boldsymbol{F}^p, \quad \bar{\varepsilon}^p, \quad d, \quad T.$$

- Conservations and thermodynamic laws:

$$\begin{aligned}
&\dot{\rho_0} = 0,\\
&\rho_0 \mathbf{a} = \boldsymbol{\nabla}\cdot\boldsymbol{P} + \rho_0 \mathbf{b},\\
&\boldsymbol{P}\boldsymbol{F} = \boldsymbol{F}\boldsymbol{P}^T,\\
&f - \boldsymbol{\nabla}\cdot\boldsymbol{\xi} = 0,\\
&\dot{u} + \dot{k} = \mathcal{P}^{\text{ext}} + \rho_0 q - \boldsymbol{\nabla}\cdot\mathbf{h},\\
&\dot{s}^{\text{int}} = \dot{s} - \frac{\rho_0 q}{T} + \boldsymbol{\nabla}\cdot\frac{\mathbf{h}}{T} \geqslant 0.
\end{aligned}$$

- Generalized forces are

$$\boldsymbol{P} = \boldsymbol{P}^{\text{eq}} + \boldsymbol{P}^{\text{vis}}, \quad \boldsymbol{T} = \boldsymbol{T}^{\text{eq}} + \boldsymbol{T}^{\text{vis}}, \quad Y = Y^{\text{eq}} + Y^{\text{vis}},$$
$$f = f^{\text{eq}} + f^{\text{vis}}, \quad \boldsymbol{\xi} = \boldsymbol{\xi}^{\text{eq}} + \boldsymbol{\xi}^{\text{vis}},$$

- Following the Coleman-Noll procedure:

$$\boldsymbol{P}^{\text{eq}} = \psi_{,\boldsymbol{F}}, \quad \boldsymbol{T}^{\text{eq}} = \psi_{,\boldsymbol{F}^p}, \quad Y^{\text{eq}} = \psi_{,\bar{\varepsilon}^p},$$
$$f^{\text{eq}} = \psi_{,d}, \quad \boldsymbol{\xi}^{\text{eq}} = \psi_{,\boldsymbol{\nabla} d}, \quad -s = \psi_{,T}.$$

- Viscous forces follow from the dual kinetic potential Δ^*:

$$\boldsymbol{P}^{\text{vis}} = \Delta^*_{,\dot{\boldsymbol{F}}}, \quad \boldsymbol{T}^{\text{vis}} = \Delta^*_{,\dot{\boldsymbol{F}}^p}, \quad Y^{\text{vis}} = \Delta^*_{,\dot{\bar{\varepsilon}}^p},$$
$$f^{\text{vis}} = \Delta^*_{,\dot{d}}, \quad \boldsymbol{\xi}^{\text{vis}} = \Delta^*_{,\boldsymbol{\nabla}\dot{d}}.$$

- To satisfy the second law:

$$\delta = \boldsymbol{P}^{\text{vis}} : \dot{\boldsymbol{F}} + \boldsymbol{T}^{\text{vis}} : \dot{\boldsymbol{F}}^p + Y^{\text{vis}}\dot{\bar{\varepsilon}}^p + f^{\text{vis}}\dot{d} + \boldsymbol{\xi}^{\text{vis}} \cdot \boldsymbol{\nabla}\dot{d} \geqslant 0.$$

With $\mathcal{V} = \{\dot{\boldsymbol{\phi}}, \dot{\boldsymbol{F}}^p, \dot{\bar{\varepsilon}}^p, \dot{d}\}$:

$$(\mathcal{V}, \dot{s}, T) = \arg\left(\inf_{\mathcal{V}, \dot{s}} \sup_{T} L\right)$$

With $\mathcal{V} = \{\dot{\boldsymbol{\phi}}, \dot{\boldsymbol{F}}^p, \dot{\bar{\varepsilon}}^p, \dot{d}\}$:

$$(\mathcal{V}, \dot{s}, T) = \arg\left(\inf_{\mathcal{V},\dot{s}} \sup_{T} L\right)$$

Benefits:

- From a theoretical standpoint:
  - The direct method of calculus of variations informs conditions for the existence and uniqueness of solutions.
  - Localization effects can be studied within the framework of free-discontinuity problems.
- From a computational standpoint:
  - Discretization leads to a symmetric operator.
  - Discretization leads to robust and efficient variational constitutive update.
  - The total potential can assist line search.
  - The total potential can be directly used as an error indicator for adaptive mesh refinement.
  - Many powerful optimization packages exist, e.g. PETSc/TAO, Trilinos, Matlab, etc..

With $\mathcal{V} = \{\dot{\boldsymbol{\phi}}, \dot{\boldsymbol{F}}^p, \dot{\bar{\varepsilon}}^p, \dot{d}\}$:

$$(\mathcal{V}, \dot{s}, T) = \arg\left(\inf_{\mathcal{V},\dot{s}} \sup_{T} L\right)$$

Benefits:

- From a theoretical standpoint:
  - The direct method of calculus of variations informs conditions for the existence and uniqueness of solutions.
  - Localization effects can be studied within the framework of free-discontinuity problems.
- From a computational standpoint:
  - Discretization leads to a symmetric operator.
  - Discretization leads to robust and efficient variational constitutive update.
  - The total potential can assist line search.
  - The total potential can be directly used as an error indicator for adaptive mesh refinement.
  - Many powerful optimization packages exist, e.g. PETSc/TAO, Trilinos, Matlab, etc..

Limitations:

- Construction of such a potential is no easy task.
- (Other limitations will be discussed in the end.)

With $\mathcal{V} = \{\dot{\boldsymbol{\phi}}, \dot{\boldsymbol{F}}^p, \dot{\bar{\varepsilon}}^p, \dot{d}\}$:

$$(\mathcal{V}, \dot{s}, T) = \arg\left(\inf_{\mathcal{V}, \dot{s}} \sup_{T} L\right)$$

Benefits:

- From a theoretical standpoint:
  - The direct method of calculus of variations informs conditions for the existence and uniqueness of solutions.
  - Localization effects can be studied within the framework of free-discontinuity problems.
- From a computational standpoint:
  - Discretization leads to a symmetric operator.
  - Discretization leads to robust and efficient variational constitutive update.
  - The total potential can assist line search.
  - The total potential can be directly used as an error indicator for adaptive mesh refinement.
  - Many powerful optimization packages exist, e.g. PETSc/TAO, Trilinos, Matlab, etc..

Limitations:

- Construction of such a potential is no easy task.
- (Other limitations will be discussed in the end.)

State-of-the-art: variational brittle fracture that concerns with

$$\boldsymbol{\phi}, \quad d,$$

while we are looking at

$$\boldsymbol{\phi}, \quad \boldsymbol{F}^p, \quad \bar{\varepsilon}^p, \quad d, \quad T.$$

The total potential L is constructed as

$$L = \int_{\Omega_0} \varphi \, \mathrm{d}V - \mathcal{P}^{\text{ext}},$$

$$\varphi = \dot{k} + \dot{u} + \Delta^* - T\dot{s} - \chi,$$

The external power expenditure $\mathcal{P}^{\text{ext}}(\dot{\boldsymbol{\phi}}, T)$ is defined as

$$\mathcal{P}^{\text{ext}} = \underbrace{\int_{\Omega_0} \rho_0 \mathbf{b} \cdot \dot{\boldsymbol{\phi}} \, \mathrm{d}V}_{\text{body force}} + \underbrace{\int_{\partial_t \Omega_0} \mathbf{t} \cdot \dot{\boldsymbol{\phi}} \, \mathrm{d}A}_{\text{surface traction}} + \underbrace{\int_{\partial_h \Omega_0} \bar{h}_n \ln\left(\frac{T}{T_0}\right) \mathrm{d}A}_{\text{external heat flux}}$$
$$+ \underbrace{\int_{\partial_r \Omega_0} h \left[T - T_0 \ln\left(\frac{T}{T_0}\right)\right] \mathrm{d}A}_{\text{external heat convection}} - \underbrace{\int_{\Omega_0} \rho_0 q \ln\left(\frac{T}{T_0}\right) \mathrm{d}V}_{\text{heat source}},$$

The total potential L is constructed as

$$L = \int_{\Omega_0} \varphi \; \mathrm{d}V - \mathcal{P}^{\mathrm{ext}},$$

$$\varphi = \dot{k} + \dot{u} + \Delta^* - T\dot{s} - \chi,$$

The external power expenditure $\mathcal{P}^{\mathrm{ext}}(\dot{\boldsymbol{\phi}}, T)$ is defined as

$$\mathcal{P}^{\mathrm{ext}} = \underbrace{\int_{\Omega_0} \rho_0 \mathbf{b} \cdot \dot{\boldsymbol{\phi}} \; \mathrm{d}V}_{\text{body force}} + \underbrace{\int_{\partial_t \Omega_0} \mathbf{t} \cdot \dot{\boldsymbol{\phi}} \; \mathrm{d}A}_{\text{surface traction}} + \underbrace{\int_{\partial_h \Omega_0} \bar{h}_n \ln\left(\frac{T}{T_0}\right) \; \mathrm{d}A}_{\text{external heat flux}}$$
$$+ \underbrace{\int_{\partial_r \Omega_0} h \left[T - T_0 \ln\left(\frac{T}{T_0}\right)\right] \; \mathrm{d}A}_{\text{external heat convection}} - \underbrace{\int_{\Omega_0} \rho_0 q \ln\left(\frac{T}{T_0}\right) \; \mathrm{d}V}_{\text{heat source}},$$

- Mass balance and angular momentum balance are satisfied by construction.
- Linear momentum balance:

$$\rho_0 \mathbf{a} = \boldsymbol{\nabla} \cdot \boldsymbol{P} + \mathbf{b}.$$

- Micro-macro force balance:

$$\boldsymbol{\nabla} \cdot \boldsymbol{\xi} - f = 0.$$

- Plastic flow:

$$\left(\dot{\boldsymbol{F}}^p, \dot{\bar{\varepsilon}}^p\right) = \arg \inf_{\dot{\boldsymbol{F}}^p, \dot{\bar{\varepsilon}}^p} \left[\boldsymbol{T}^{\mathrm{eq}} : \dot{\boldsymbol{F}}^p + Y^{\mathrm{eq}} \dot{\bar{\varepsilon}}^p + \Delta^*\right]$$
$$\text{subject to} \quad \boldsymbol{L}(\boldsymbol{Z})\dot{\boldsymbol{Z}} = \boldsymbol{0}.$$

- Heat transfer:

$$T\dot{s} = \rho_0 q - \boldsymbol{\nabla} \cdot \mathbf{h} + \delta.$$

- (Strict) dissipation inequality requires Δ^* to be convex in each rate.

Introduction
Background
Phase-field approach to fracture

The Variational Framework
Thermodynamics
The variational statement

Numerical Examples and Applications
Towards Ductile Fracture
Intergranular Fracture in Polycrystalline Materials
Soil Desiccation

Conclusions and Future Work

Acknowledgements

References

Introduction
Background
Phase-field approach to fracture
The Variational Framework
Thermodynamics
The variational statement
Numerical Examples and Applications
Towards Ductile Fracture
Intergranular Fracture in Polycrystalline Materials
Soil Desiccation
Conclusions and Future Work
Acknowledgements
References

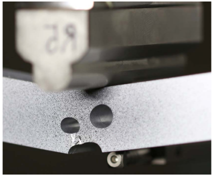

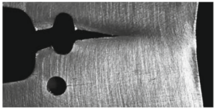

There exist many approaches to modeling plasticity in the context of phase-field fracture [2, 3, 4, 5, 6, 7, 8, 9].

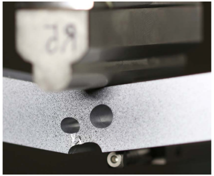
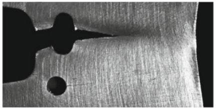


There exist many approaches to modeling plasticity in the context of phase-field fracture [2, 3, 4, 5, 6, 7, 8, 9].

How to best design the coupling between plasticity and fracture remains an open question. Some challenges/issues:

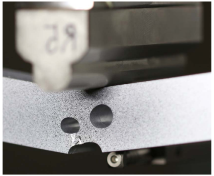

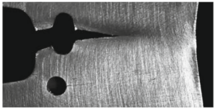

There exist many approaches to modeling plasticity in the context of phase-field fracture [2, 3, 4, 5, 6, 7, 8, 9].

How to best design the coupling between plasticity and fracture remains an open question. Some challenges/issues:

- Fracture tends to propagate along the plastic zone.

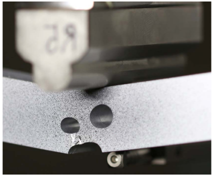

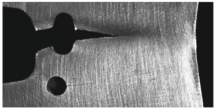

There exist many approaches to modeling plasticity in the context of phase-field fracture [2, 3, 4, 5, 6, 7, 8, 9].

How to best design the coupling between plasticity and fracture remains an open question. Some challenges/issues:

- Fracture tends to propagate along the plastic zone.
- Most existing models
  - are not variational,

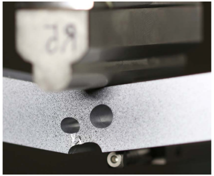

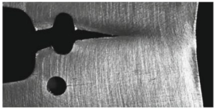

There exist many approaches to modeling plasticity in the context of phase-field fracture [2, 3, 4, 5, 6, 7, 8, 9].

How to best design the coupling between plasticity and fracture remains an open question. Some challenges/issues:

- Fracture tends to propagate along the plastic zone.
- Most existing models
  - are not variational,
  - require re-calibration of material parameters,

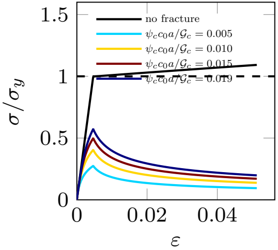

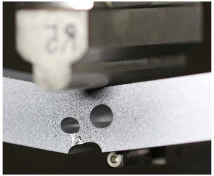

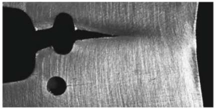

There exist many approaches to modeling plasticity in the context of phase-field fracture [2, 3, 4, 5, 6, 7, 8, 9].

How to best design the coupling between plasticity and fracture remains an open question. Some challenges/issues:

- Fracture tends to propagate along the plastic zone.
- Most existing models
  - are not variational,
  - require re-calibration of material parameters,
  - result in regularization-dependent response.

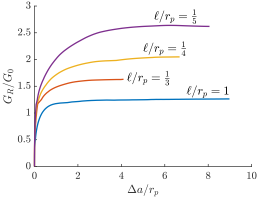

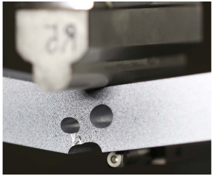

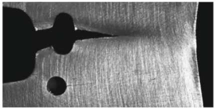

There exist many approaches to modeling plasticity in the context of phase-field fracture [2, 3, 4, 5, 6, 7, 8, 9].

How to best design the coupling between plasticity and fracture remains an open question. Some challenges/issues:

- Fracture tends to propagate along the plastic zone.
- Most existing models
  - are not variational,
  - require re-calibration of material parameters,
  - result in regularization-dependent response.
- How much plastic work contributes to fracture evolution?

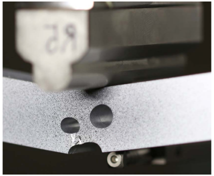

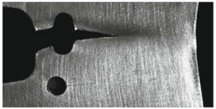

There exist many approaches to modeling plasticity in the context of phase-field fracture [2, 3, 4, 5, 6, 7, 8, 9].

How to best design the coupling between plasticity and fracture remains an open question. Some challenges/issues:

- Fracture tends to propagate along the plastic zone.
- Most existing models
  - are not variational,
  - require re-calibration of material parameters,
  - result in regularization-dependent response.
- How much plastic work contributes to fracture evolution?
- How much plastic work converts to heat generation?

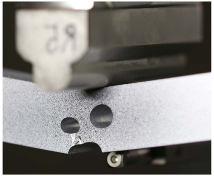
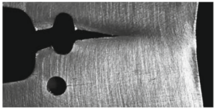


There exist many approaches to modeling plasticity in the context of phase-field fracture [2, 3, 4, 5, 6, 7, 8, 9].

How to best design the coupling between plasticity and fracture remains an open question. Some challenges/issues:

- Fracture tends to propagate along the plastic zone.
- Most existing models
  - are not variational,
  - require re-calibration of material parameters,
  - result in regularization-dependent response.
- How much plastic work contributes to fracture evolution?
- How much plastic work converts to heat generation?

All of the issues above can be addressed by the proposed framework (with proper constitutive choices).

$$L = \int_{\Omega_0} \left[\dot{\psi}^e + \psi^{e*} + (1-\mathcal{Q})\dot{\psi}^p + \mathcal{Q}\psi^{p*} + \dot{\psi}^f + \psi^{f*} - T\dot{s} - \chi \right] \mathrm{d}V - \mathcal{P}^{\mathrm{ext}},$$

subject to $\boldsymbol{L}(\boldsymbol{Z})\dot{\boldsymbol{Z}} = \boldsymbol{0}$.

Option 1 (Compressible Neo-Hookean):

$$\begin{aligned}
\psi^e &= g^e \psi^e_{\langle A \rangle} + \psi^e_{\langle I \rangle}, \\
\psi^e_{\langle A \rangle} &= \mathbb{H}_1(J) \left\{ \frac{1}{2} K \left[\frac{1}{2}(J^2 - 1) - \ln(J) \right] \right\} \\
&\quad + \frac{1}{2} G \left(\overline{\boldsymbol{C}} : \boldsymbol{C}^{p\,-1} - 3 \right), \\
\psi^e_{\langle I \rangle} &= (1 - \mathbb{H}_1(J)) \left\{ \frac{1}{2} K \left[\frac{1}{2}(J^2 - 1) - \ln(J) \right] \right\}.
\end{aligned}$$

Option 2 (Hencky):

$$\begin{aligned}
\psi^e &= g^e \psi^e_{\langle A \rangle} + \psi^e_{\langle I \rangle}, \\
\psi^e_{\langle A \rangle} &= \frac{1}{2} K \left\langle \mathrm{tr}(\boldsymbol{\varepsilon}^e) \right\rangle_+^2 + G \, \mathrm{dev}\, \boldsymbol{\varepsilon}^e : \mathrm{dev}\, \boldsymbol{\varepsilon}^e, \\
\psi^e_{\langle I \rangle} &= \frac{1}{2} K \left\langle \mathrm{tr}(\boldsymbol{\varepsilon}^e) \right\rangle_-^2, \\
\boldsymbol{\varepsilon}^e &= \frac{1}{2} \ln \left(\boldsymbol{C}^e \right).
\end{aligned}$$

$$L = \int_{\Omega_0} \left[\dot{\psi}^e + \psi^{e*} + (1 - \mathcal{Q})\dot{\psi}^p + \mathcal{Q}\psi^{p*} + \dot{\psi}^f + \psi^{f*} - T\dot{s} - \chi \right] \, \mathrm{d}V - \mathcal{P}^{\mathrm{ext}},$$

$$\text{subject to } \boldsymbol{L}(\boldsymbol{Z})\dot{\boldsymbol{Z}} = \boldsymbol{0}.$$

Newtonian viscosity:

$$\psi^{e*} = g^e J \left[\frac{1}{2}\zeta \, \mathrm{tr}(\boldsymbol{d})^2 + \eta \boldsymbol{d} : \boldsymbol{d} \right],$$

$$\boldsymbol{d} = \mathrm{sym}\left(\dot{\boldsymbol{F}}\boldsymbol{F}^{-1} \right).$$

$$L = \int_{\Omega_0} \left[\dot{\psi}^e + \psi^{e*} + (1-\mathcal{Q})\dot{\psi}^p + \mathcal{Q}\psi^{p*} + \dot{\psi}^f + \psi^{f*} - T\dot{s} - \chi \right] \, \mathrm{d}V - \mathcal{P}^{\mathrm{ext}},$$

subject to $\boldsymbol{L}(\boldsymbol{Z})\dot{\boldsymbol{Z}} = \boldsymbol{0}$.

Flow rule constraints:

$$\operatorname{tr}\left(\dot{\boldsymbol{F}}^p \boldsymbol{F}^{p-1}\right) = 0,$$

$$\left\|\dot{\boldsymbol{F}}^p \boldsymbol{F}^{p-1}\right\|^2 - \frac{3}{2}\left|\dot{\bar{\varepsilon}}^p\right|^2 = 0.$$

Remark (Flow rule)

It recovers the Prandtl-Reuss flow rule:

$$\dot{\boldsymbol{F}}^p \boldsymbol{F}^{p-1} = \dot{\bar{\varepsilon}}^p \boldsymbol{N}^p, \quad \boldsymbol{N}^p = \sqrt{\frac{3}{2}} \frac{\operatorname{dev}(\boldsymbol{M})}{\|\operatorname{dev}(\boldsymbol{M})\|},$$

and the loading/unloading conditions:

$$\phi^p \leqslant 0, \quad \dot{\bar{\varepsilon}}^p \geqslant 0, \quad \phi^p \dot{\bar{\varepsilon}}^p = 0,$$

$$\phi^p = \|\operatorname{dev}(\boldsymbol{M})\| - \sqrt{\frac{2}{3}}\left(Y^{\mathrm{eq}} + Y^{\mathrm{vis}}\right).$$

$$L = \int_{\Omega_0} \left[\dot{\psi}^e + \psi^{e*} + (1-\mathcal{Q})\dot{\psi}^p + \mathcal{Q}\psi^{p*} + \dot{\psi}^f + \psi^{f*} - T\dot{s} - \chi \right] \mathrm{d}V - \mathcal{P}^{\mathrm{ext}},$$

subject to $\boldsymbol{L}(\boldsymbol{Z})\dot{\boldsymbol{Z}} = \boldsymbol{0}$.

Option 1 (Linear hardening):

$$\psi^p = g^p \left(\sigma_y \bar{\varepsilon}^p + \frac{1}{2} H \bar{\varepsilon}^{p\,2} \right),$$
$$\psi^{p*} = g^p (\sigma_y + H\bar{\varepsilon}^p)\dot{\bar{\varepsilon}}^p.$$

Option 2 (Power-law hardening):

$$\psi^p = g^p \frac{n}{n+1} \sigma_y \epsilon_0 \left[\left(1 + \frac{\bar{\varepsilon}^p}{\epsilon_0} \right)^{(n+1)/n} - 1 \right],$$
$$\psi^{p*} = g^p \sigma_y \left(1 + \frac{\bar{\varepsilon}^p}{\epsilon_0} \right)^{1/n} \dot{\bar{\varepsilon}}^p.$$

Option 3 (Perfect plasticity with thermal softening):

$$\psi^p = g^p \sigma_y^T \bar{\varepsilon}^p, \quad \psi^{p*} = g^p \sigma_y^T \dot{\bar{\varepsilon}}^p,$$
$$\sigma_y^T = \frac{\sigma_0}{\exp\left(-\frac{Q}{RT} \right)}$$

Remark (The Taylor-Quinney factor)

Due to thermal softening (option 3), to get an increase in temperature from plastic dissipation:

$$\frac{Q}{Q+RT} \leqslant \mathcal{Q} \leqslant 1.$$

$$L = \int_{\Omega_0} \left[\dot{\psi}^e + \psi^{e*} + (1-\mathcal{Q})\dot{\psi}^p + \mathcal{Q}\psi^{p*} + \dot{\psi}^f + \psi^{f*} - T\dot{s} - \chi \right] \, \mathrm{d}V - \mathcal{P}^{\mathrm{ext}},$$

subject to $\boldsymbol{L}(\boldsymbol{Z})\dot{\boldsymbol{Z}} = \boldsymbol{0}$.

Fracture energy density:

$$\psi^f = \frac{\mathcal{G}_c}{c_0 l}\left(C\alpha + l^2 \boldsymbol{\nabla} d \cdot \boldsymbol{\nabla} d\right).$$

Viscous regularization and coalescence dissipation:

$$\psi^{f*} = \frac{1}{2} v\dot{d}^2 + (1-C)\frac{\mathcal{G}_c}{c_0 l}\alpha_{,d}\dot{d} - (1-\beta)\frac{\mathcal{G}_c}{c_0 l}\alpha_{,d}\left(1 - e^{-\bar{\varepsilon}^p/\varepsilon_0}\right)\dot{d}.$$

Irreversibility constraint:

$$\dot{d} \geqslant 0.$$

Remark

The contributions from plasticity is clear in the fracture envelope:

$$v\dot{d} = \boldsymbol{\nabla} \cdot \frac{2\mathcal{G}_c l}{c_0} \boldsymbol{\nabla} d - \left(\frac{\widehat{\mathcal{G}_c}}{c_0 l}\alpha_{,d} + \psi^d \right),$$

$$\psi^d = \psi^e_{,d} + (1-\mathcal{Q})\psi^p_{,d},$$

$$\widehat{\mathcal{G}_c} = g^c \mathcal{G}_c, \quad g^c = 1 - (1-\beta)\left(1 - e^{-\bar{\varepsilon}^p/\varepsilon_0}\right),$$

Remark

To satisfy the second law: $0 < C \leqslant \beta$.

$$L = \int_{\Omega_0} \left[\dot{\psi}^e + \psi^{e*} + (1-\mathcal{Q})\dot{\psi}^p + \mathcal{Q}\psi^{p*} + \dot{\psi}^f + \psi^{f*} - T\dot{s} - {\color{red}\chi} \right] \, \mathrm{d}V - \mathcal{P}^{\mathrm{ext}},$$

$$\text{subject to } \boldsymbol{L}(\boldsymbol{Z})\dot{\boldsymbol{Z}} = \boldsymbol{0}.$$

Fourier potential:

$$\chi = \frac{1}{2}\kappa \mathbf{g} \cdot \mathbf{g},$$
$$\mathbf{g} = -\boldsymbol{\nabla} T / T.$$

Remark

The heat conduction equation can be written as

$$\rho_0 c_v \dot{T} = \rho_0 q + \boldsymbol{\nabla} \cdot \kappa \boldsymbol{\nabla} T + \delta + \delta_T,$$
$$\delta = \boldsymbol{P}^{\mathrm{vis}} : \dot{\boldsymbol{F}} + Y^{\mathrm{vis}} \dot{\bar{\varepsilon}}^p + f^{\mathrm{vis}} \dot{d},$$
$$\delta_T = -g^p (1-\mathcal{Q}) \frac{Q}{RT} \sigma_y^T \dot{\bar{\varepsilon}}^p.$$

How to best design the coupling between plasticity and fracture remains an open question. Some challenges/issues:

- Fracture tends to propagate along the plastic zone.
- Most existing models
  - are not variational,
  - require re-calibration of material parameters,
  - result in regularization-dependent response.
- How much plastic work contributes to fracture evolution?
- How much plastic work converts to heat generation?

How to best design the coupling between plasticity and fracture remains an open question. Some challenges/issues:

- ~~Fracture tends to propagate along the plastic zone.~~
- Most existing models
  - are not variational,
  - require re-calibration of material parameters,
  - result in regularization-dependent response.
- How much plastic work contributes to fracture evolution?
- How much plastic work converts to heat generation?

How to best design the coupling between plasticity and fracture remains an open question. Some challenges/issues:

- ~~Fracture tends to propagate along the plastic zone.~~
- Most existing models
  - ~~are not variational,~~
  - require re-calibration of material parameters,
  - result in regularization-dependent response.
- How much plastic work contributes to fracture evolution?
- How much plastic work converts to heat generation?

How to best design the coupling between plasticity and fracture remains an open question. Some challenges/issues:

- ~~Fracture tends to propagate along the plastic zone.~~
- Most existing models
  - ~~are not variational,~~
  - require re-calibration of material parameters,
  - result in regularization-dependent response.
- How much plastic work contributes to fracture evolution?
- How much plastic work converts to heat generation?

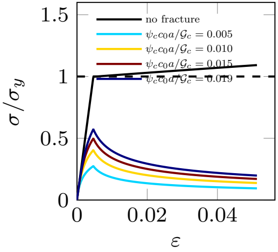

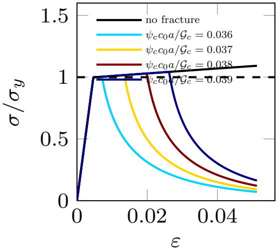

How to best design the coupling between plasticity and fracture remains an open question. Some challenges/issues:

- ~~Fracture tends to propagate along the plastic zone.~~
- Most existing models
  - ~~are not variational,~~
  - ~~require re-calibration of material parameters,~~
  - result in regularization-dependent response.
- How much plastic work contributes to fracture evolution?
- How much plastic work converts to heat generation?

How to best design the coupling between plasticity and fracture remains an open question. Some challenges/issues:

- ~~Fracture tends to propagate along the plastic zone.~~
- Most existing models
  - ~~are not variational,~~
  - ~~require re-calibration of material parameters,~~
  - result in regularization-dependent response.
- How much plastic work contributes to fracture evolution?
- How much plastic work converts to heat generation?

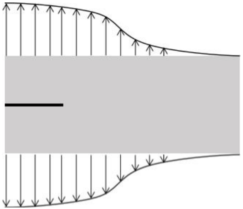

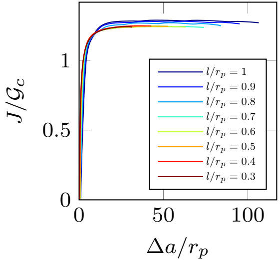

How to best design the coupling between plasticity and fracture remains an open question. Some challenges/issues:

- ~~Fracture tends to propagate along the plastic zone.~~
- ~~Most existing models~~
  - ~~are not variational,~~
  - ~~require re-calibration of material parameters,~~
  - ~~result in regularization-dependent response.~~
- How much plastic work contributes to fracture evolution?
- How much plastic work converts to heat generation?

How to best design the coupling between plasticity and fracture remains an open question. Some challenges/issues:

- ~~Fracture tends to propagate along the plastic zone.~~
- ~~Most existing models~~
  - ~~are not variational,~~
  - ~~require re-calibration of material parameters,~~
  - ~~result in regularization-dependent response.~~
- ~~How much plastic work contributes to fracture evolution?~~
- ~~How much plastic work converts to heat generation?~~

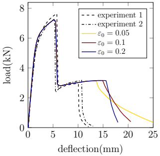

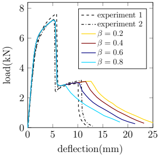

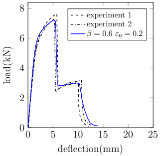

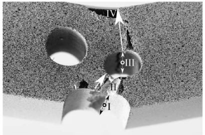

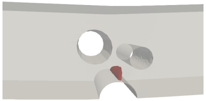

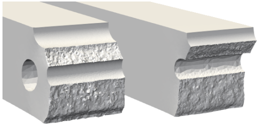

- A three-point bending experiment is simulated.
- The aluminum specimen is modeled as a compressible Neo-Hookean material, with linear hardening, $\mathcal{Q} = 1$.
- Coalescence dissipation is included. The effects of β and ε_0 are investigated in a 2D setting.
- Parameters are calibrated based on a tensile tension test.
- “Shear lips” are not captured by numerical simulations.
- Crack paths and load deflection curves have excellent agreement with the experiment.

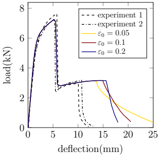

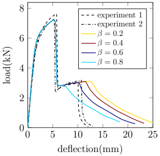

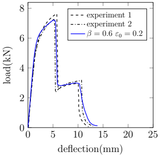

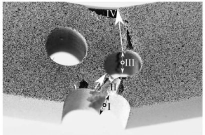

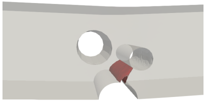

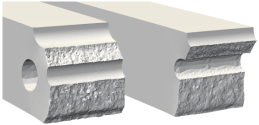

- A three-point bending experiment is simulated.
- The aluminum specimen is modeled as a compressible Neo-Hookean material, with linear hardening, $\mathcal{Q} = 1$.
- Coalescence dissipation is included. The effects of β and ε_0 are investigated in a 2D setting.
- Parameters are calibrated based on a tensile tension test.
- “Shear lips” are not captured by numerical simulations.
- Crack paths and load deflection curves have excellent agreement with the experiment.

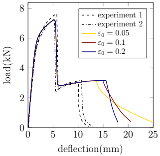

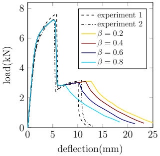

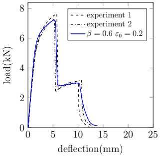

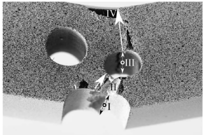

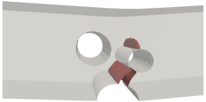

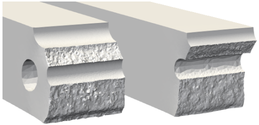

- A three-point bending experiment is simulated.
- The aluminum specimen is modeled as a compressible Neo-Hookean material, with linear hardening, $\mathcal{Q} = 1$.
- Coalescence dissipation is included. The effects of β and ε_0 are investigated in a 2D setting.
- Parameters are calibrated based on a tensile tension test.
- “Shear lips” are not captured by numerical simulations.
- Crack paths and load deflection curves have excellent agreement with the experiment.

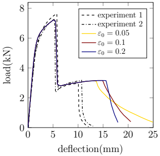

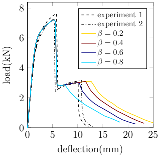

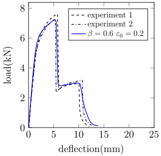

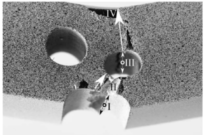

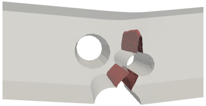

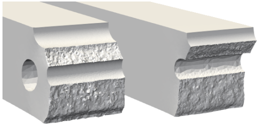

- A three-point bending experiment is simulated.
- The aluminum specimen is modeled as a compressible Neo-Hookean material, with linear hardening, $\mathcal{Q} = 1$.
- Coalescence dissipation is included. The effects of β and ε_0 are investigated in a 2D setting.
- Parameters are calibrated based on a tensile tension test.
- "Shear lips" are not captured by numerical simulations.
- Crack paths and load deflection curves have excellent agreement with the experiment.

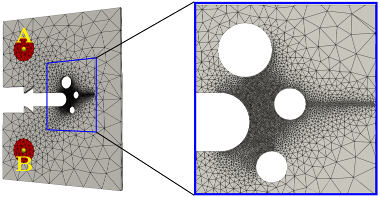

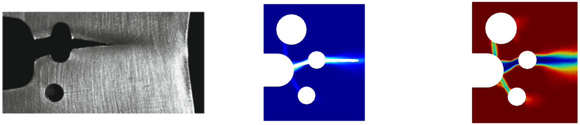

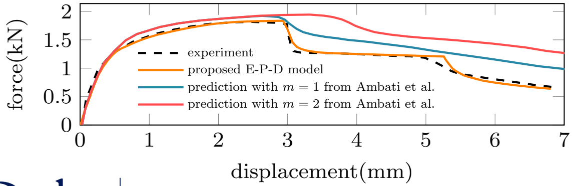

- A recent Sandia Fracture Challenge.
- Material properties are calibrated using provided tensile tension test data.
- Loading pins A and B are modeled as purely elastic materials with the same constants as the specimen.
- The predicted force-displacement curve is compared with the experimental data and predictions by other existing phase-field models of ductile fracture.
- The agreement between the experiment and our simulation is remarkable, both in terms of the crack path and the force-displacement curve.

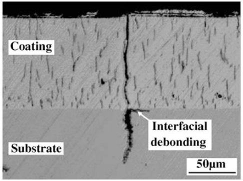

Background:

- High temperature heat exchangers are key components of many power conversion systems, including advanced nuclear power generation systems.
- They operate in the inlet temperature range of 750-1100 °C and are subject to unique operating challenges including oxidation, corrosion, creep and fracture.

Model:

- To model energy release associated with debonding:

$$\psi^f = \frac{\mathcal{G}_c}{c_0 l}\left(C\alpha(d) + l^2 \nabla d \cdot \nabla d\right) + \frac{1}{\tau}\mathcal{G}\omega(c).$$

- A lower dimensional representation of the oxide layer:

$$\psi^e = g^e_{\text{ip}}\psi^e_{\text{ip},\langle A\rangle} + \psi^e_{\text{ip},\langle I\rangle} + g^e_{\text{op}}\psi^e_{\text{op},\langle A\rangle} + \psi^e_{\text{ip},\langle I\rangle}.$$

- The perfect plasticity model with thermal softening is approximated using a power-law creep model:

$$\dot{\bar{\varepsilon}}^p = A\left(\frac{\bar{\sigma}}{g^p\sigma_0}\right)^n \exp\left(-\frac{nQ}{RT}\right).$$

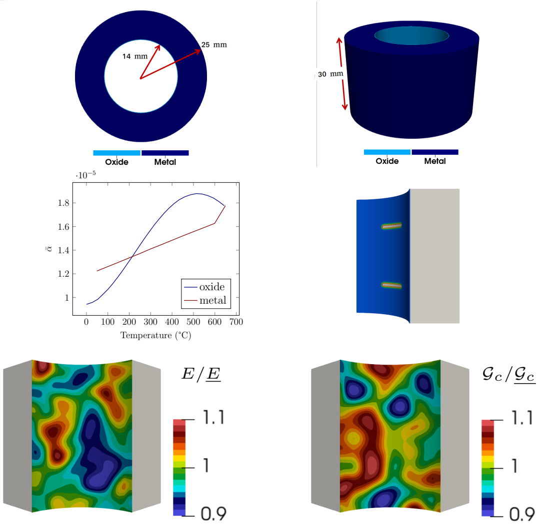

- The HTHX is simulated for 180 days under normal operating conditions, followed by a shutdown (6-hour transition).
- The HTHX is surround by high temperature pressurized fluids during normal operation. The temperature and the pressure of the fluids drop after shutting down.
- Most model parameters are adopted from [10].
- Creep deformation accumulates under normal operating conditions. The effective creep strain localizes around the cracks.
- Debonding occurs at weaker locations in the vicinity of the crack surfaces.
- Transverse cracks nucleate and propagate while shutting down.

Case I: Initial transverse cracks

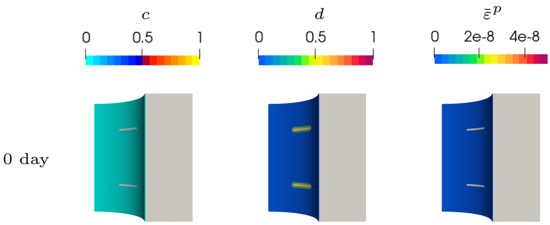

- The HTHX is simulated for 180 days under normal operating conditions, followed by a shutdown (6-hour transition).
- The HTHX is surround by high temperature pressurized fluids during normal operation. The temperature and the pressure of the fluids drop after shutting down.
- Most model parameters are adopted from [10].
- Creep deformation accumulates under normal operating conditions. The effective creep strain localizes around the cracks.
- Debonding occurs at weaker locations in the vicinity of the crack surfaces.
- Transverse cracks nucleate and propagate while shutting down.

Case I: Initial transverse cracks

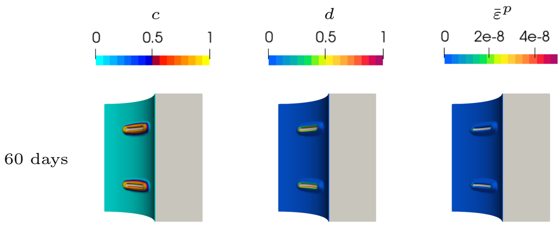

- The HTHX is simulated for 180 days under normal operating conditions, followed by a shutdown (6-hour transition).
- The HTHX is surround by high temperature pressurized fluids during normal operation. The temperature and the pressure of the fluids drop after shutting down.
- Most model parameters are adopted from [10].
- Creep deformation accumulates under normal operating conditions. The effective creep strain localizes around the cracks.
- Debonding occurs at weaker locations in the vicinity of the crack surfaces.
- Transverse cracks nucleate and propagate while shutting down.

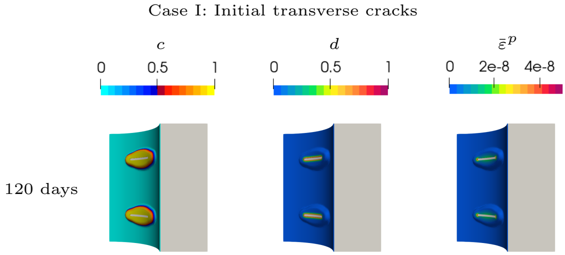

- The HTHX is simulated for 180 days under normal operating conditions, followed by a shutdown (6-hour transition).
- The HTHX is surround by high temperature pressurized fluids during normal operation. The temperature and the pressure of the fluids drop after shutting down.
- Most model parameters are adopted from [10].
- Creep deformation accumulates under normal operating conditions. The effective creep strain localizes around the cracks.
- Debonding occurs at weaker locations in the vicinity of the crack surfaces.
- Transverse cracks nucleate and propagate while shutting down.

Case I: Initial transverse cracks

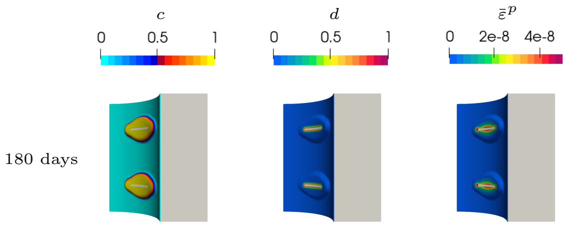

- The HTHX is simulated for 180 days under normal operating conditions, followed by a shutdown (6-hour transition).
- The HTHX is surround by high temperature pressurized fluids during normal operation. The temperature and the pressure of the fluids drop after shutting down.
- Most model parameters are adopted from [10].
- Creep deformation accumulates under normal operating conditions. The effective creep strain localizes around the cracks.
- Debonding occurs at weaker locations in the vicinity of the crack surfaces.
- Transverse cracks nucleate and propagate while shutting down.

Case I: Initial transverse cracks

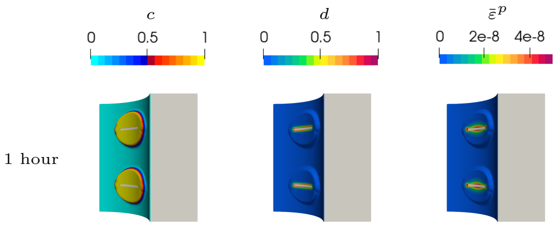

- The HTHX is simulated for 180 days under normal operating conditions, followed by a shutdown (6-hour transition).
- The HTHX is surround by high temperature pressurized fluids during normal operation. The temperature and the pressure of the fluids drop after shutting down.
- Most model parameters are adopted from [10].
- Creep deformation accumulates under normal operating conditions. The effective creep strain localizes around the cracks.
- Debonding occurs at weaker locations in the vicinity of the crack surfaces.
- Transverse cracks nucleate and propagate while shutting down.

Case I: Initial transverse cracks

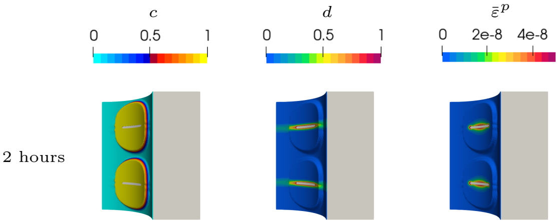

- The HTHX is simulated for 180 days under normal operating conditions, followed by a shutdown (6-hour transition).
- The HTHX is surround by high temperature pressurized fluids during normal operation. The temperature and the pressure of the fluids drop after shutting down.
- Most model parameters are adopted from [10].
- Creep deformation accumulates under normal operating conditions. The effective creep strain localizes around the cracks.
- Debonding occurs at weaker locations in the vicinity of the crack surfaces.
- Transverse cracks nucleate and propagate while shutting down.

Case I: Initial transverse cracks

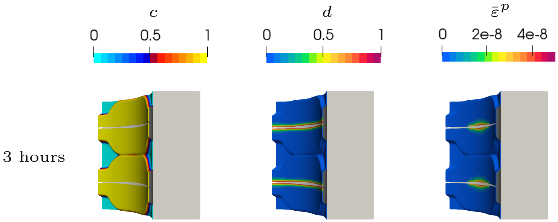

- The HTHX is simulated for 180 days under normal operating conditions, followed by a shutdown (6-hour transition).
- The HTHX is surround by high temperature pressurized fluids during normal operation. The temperature and the pressure of the fluids drop after shutting down.
- Most model parameters are adopted from [10].
- Creep deformation accumulates under normal operating conditions. The effective creep strain localizes around the cracks.
- Debonding occurs at weaker locations in the vicinity of the crack surfaces.
- Transverse cracks nucleate and propagate while shutting down.

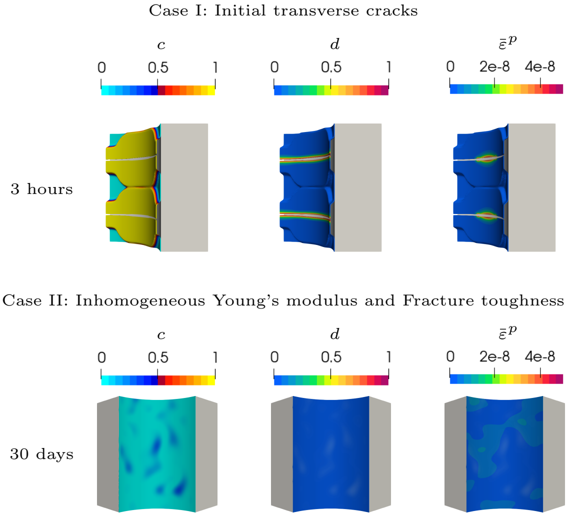

- The HTHX is simulated for 180 days under normal operating conditions, followed by a shutdown (6-hour transition).
- The HTHX is surround by high temperature pressurized fluids during normal operation. The temperature and the pressure of the fluids drop after shutting down.
- Most model parameters are adopted from [10].
- Creep deformation accumulates under normal operating conditions. The effective creep strain localizes around the cracks.
- Debonding occurs at weaker locations in the vicinity of the crack surfaces.
- Transverse cracks nucleate and propagate while shutting down.

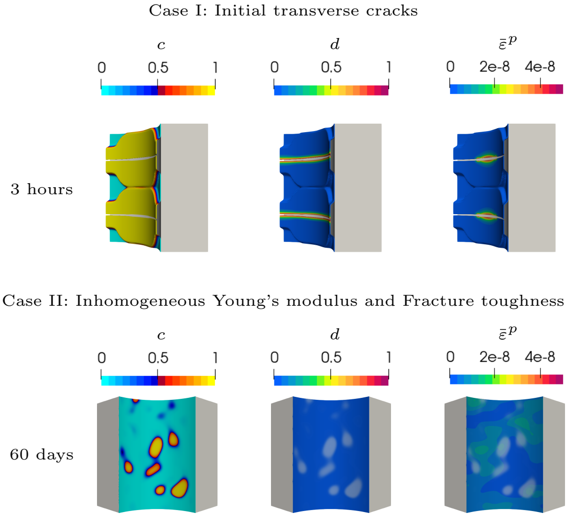

- The HTHX is simulated for 180 days under normal operating conditions, followed by a shutdown (6-hour transition).
- The HTHX is surround by high temperature pressurized fluids during normal operation. The temperature and the pressure of the fluids drop after shutting down.
- Most model parameters are adopted from [10].
- Creep deformation accumulates under normal operating conditions. The effective creep strain localizes around the cracks.
- Debonding occurs at weaker locations in the vicinity of the crack surfaces.
- Transverse cracks nucleate and propagate while shutting down.

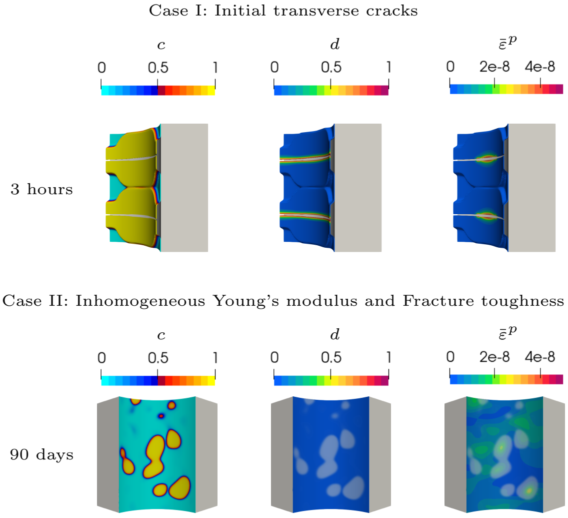

- The HTHX is simulated for 180 days under normal operating conditions, followed by a shutdown (6-hour transition).
- The HTHX is surround by high temperature pressurized fluids during normal operation. The temperature and the pressure of the fluids drop after shutting down.
- Most model parameters are adopted from [10].
- Creep deformation accumulates under normal operating conditions. The effective creep strain localizes around the cracks.
- Debonding occurs at weaker locations in the vicinity of the crack surfaces.
- Transverse cracks nucleate and propagate while shutting down.

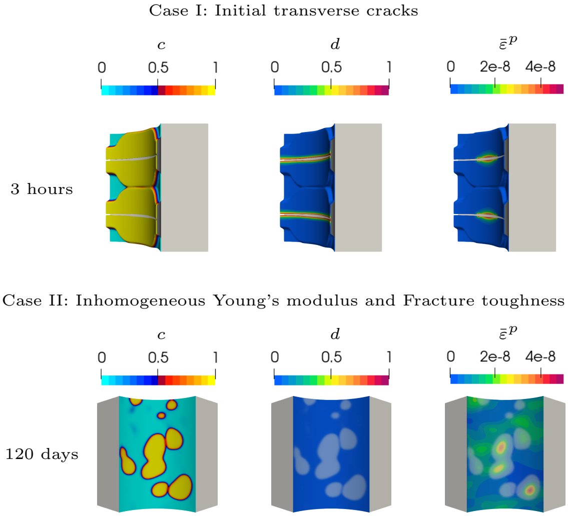

- The HTHX is simulated for 180 days under normal operating conditions, followed by a shutdown (6-hour transition).
- The HTHX is surround by high temperature pressurized fluids during normal operation. The temperature and the pressure of the fluids drop after shutting down.
- Most model parameters are adopted from [10].
- Creep deformation accumulates under normal operating conditions. The effective creep strain localizes around the cracks.
- Debonding occurs at weaker locations in the vicinity of the crack surfaces.
- Transverse cracks nucleate and propagate while shutting down.

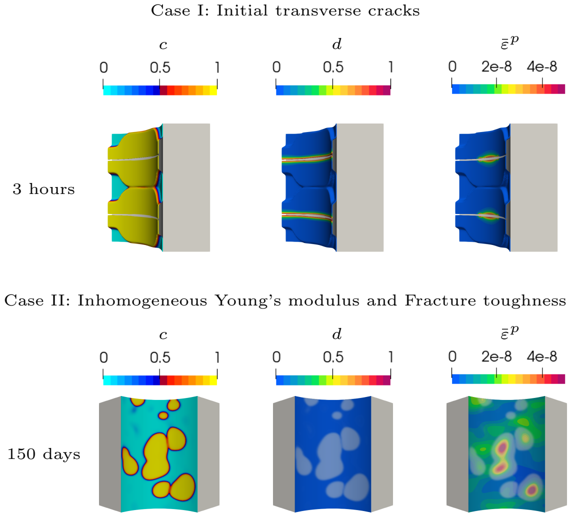

- The HTHX is simulated for 180 days under normal operating conditions, followed by a shutdown (6-hour transition).
- The HTHX is surround by high temperature pressurized fluids during normal operation. The temperature and the pressure of the fluids drop after shutting down.
- Most model parameters are adopted from [10].
- Creep deformation accumulates under normal operating conditions. The effective creep strain localizes around the cracks.
- Debonding occurs at weaker locations in the vicinity of the crack surfaces.
- Transverse cracks nucleate and propagate while shutting down.

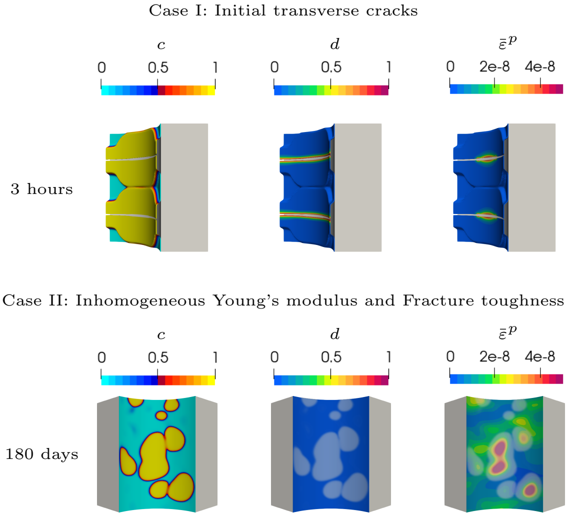

- The HTHX is simulated for 180 days under normal operating conditions, followed by a shutdown (6-hour transition).
- The HTHX is surround by high temperature pressurized fluids during normal operation. The temperature and the pressure of the fluids drop after shutting down.
- Most model parameters are adopted from [10].
- Creep deformation accumulates under normal operating conditions. The effective creep strain localizes around the cracks.
- Debonding occurs at weaker locations in the vicinity of the crack surfaces.
- Transverse cracks nucleate and propagate while shutting down.

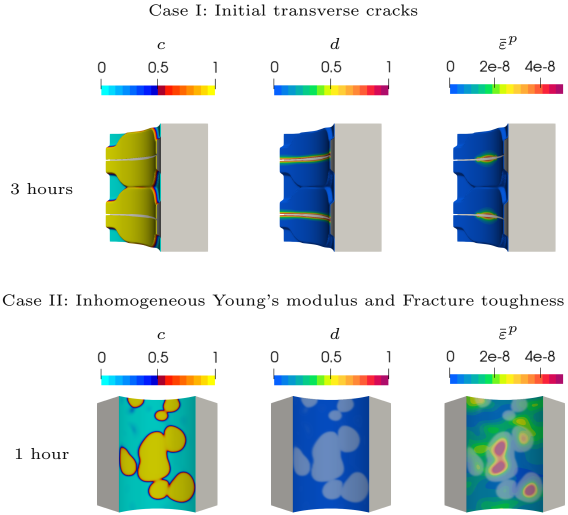

- The HTHX is simulated for 180 days under normal operating conditions, followed by a shutdown (6-hour transition).
- The HTHX is surround by high temperature pressurized fluids during normal operation. The temperature and the pressure of the fluids drop after shutting down.
- Most model parameters are adopted from [10].
- Creep deformation accumulates under normal operating conditions. The effective creep strain localizes around the cracks.
- Debonding occurs at weaker locations in the vicinity of the crack surfaces.
- Transverse cracks nucleate and propagate while shutting down.

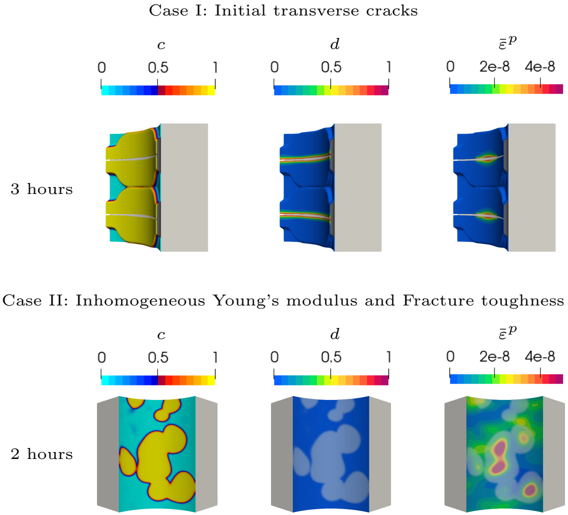

- The HTHX is simulated for 180 days under normal operating conditions, followed by a shutdown (6-hour transition).
- The HTHX is surround by high temperature pressurized fluids during normal operation. The temperature and the pressure of the fluids drop after shutting down.
- Most model parameters are adopted from [10].
- Creep deformation accumulates under normal operating conditions. The effective creep strain localizes around the cracks.
- Debonding occurs at weaker locations in the vicinity of the crack surfaces.
- Transverse cracks nucleate and propagate while shutting down.

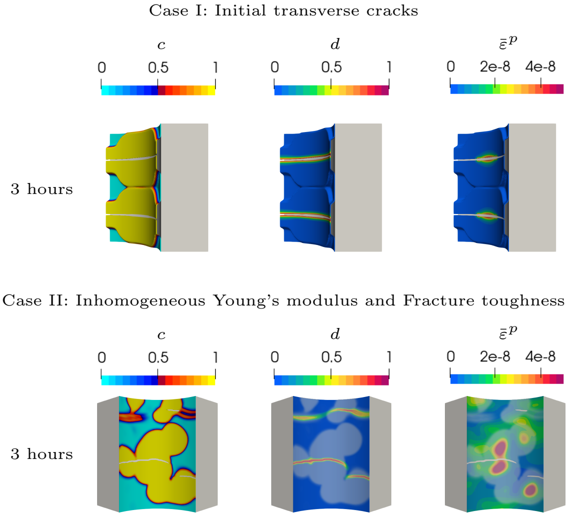

- The HTHX is simulated for 180 days under normal operating conditions, followed by a shutdown (6-hour transition).
- The HTHX is surround by high temperature pressurized fluids during normal operation. The temperature and the pressure of the fluids drop after shutting down.
- Most model parameters are adopted from [10].
- Creep deformation accumulates under normal operating conditions. The effective creep strain localizes around the cracks.
- Debonding occurs at weaker locations in the vicinity of the crack surfaces.
- Transverse cracks nucleate and propagate while shutting down.

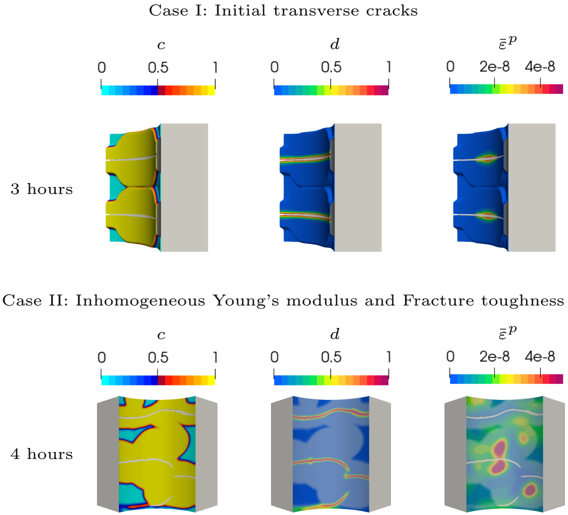

- The HTHX is simulated for 180 days under normal operating conditions, followed by a shutdown (6-hour transition).
- The HTHX is surround by high temperature pressurized fluids during normal operation. The temperature and the pressure of the fluids drop after shutting down.
- Most model parameters are adopted from [10].
- Creep deformation accumulates under normal operating conditions. The effective creep strain localizes around the cracks.
- Debonding occurs at weaker locations in the vicinity of the crack surfaces.
- Transverse cracks nucleate and propagate while shutting down.

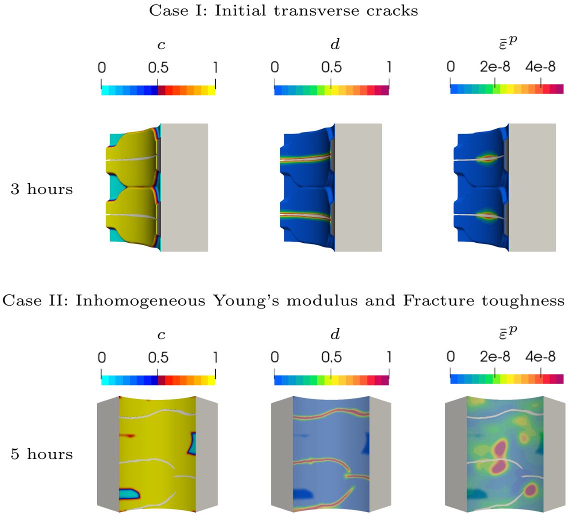

- The HTHX is simulated for 180 days under normal operating conditions, followed by a shutdown (6-hour transition).
- The HTHX is surround by high temperature pressurized fluids during normal operation. The temperature and the pressure of the fluids drop after shutting down.
- Most model parameters are adopted from [10].
- Creep deformation accumulates under normal operating conditions. The effective creep strain localizes around the cracks.
- Debonding occurs at weaker locations in the vicinity of the crack surfaces.
- Transverse cracks nucleate and propagate while shutting down.

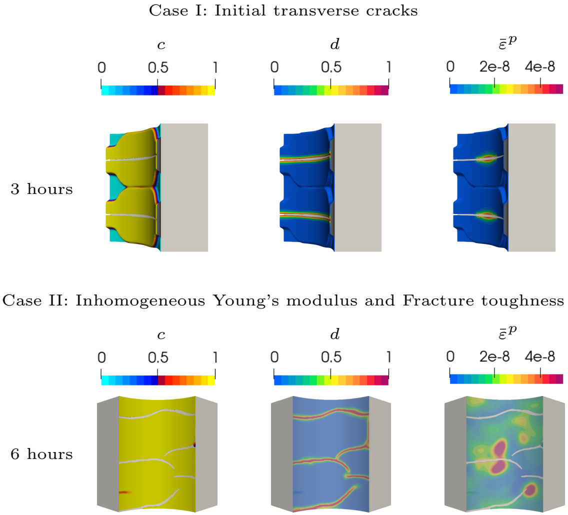

- The HTHX is simulated for 180 days under normal operating conditions, followed by a shutdown (6-hour transition).
- The HTHX is surround by high temperature pressurized fluids during normal operation. The temperature and the pressure of the fluids drop after shutting down.
- Most model parameters are adopted from [10].
- Creep deformation accumulates under normal operating conditions. The effective creep strain localizes around the cracks.
- Debonding occurs at weaker locations in the vicinity of the crack surfaces.
- Transverse cracks nucleate and propagate while shutting down.

Introduction
Background
Phase-field approach to fracture
The Variational Framework
Thermodynamics
The variational statement
Numerical Examples and Applications
Towards Ductile Fracture
Intergranular Fracture in Polycrystalline Materials
Soil Desiccation
Conclusions and Future Work
Acknowledgements
References

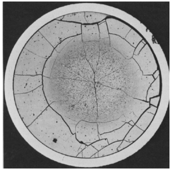 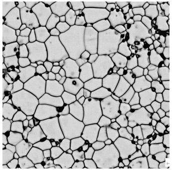

Background:

- Fission of UO_2 produces a variety of fission products.
- Properties of UO_2 are strongly influenced by fracture.
- Gas bubbles, grains, and grain boundaries alter fracture properties.
- Existing 2D models over-simplifies the microstructure and results in inaccurate strength-porosity relations.

Model:

- Helmholtz free energy density:

$$\psi = \psi^e + \psi^f.$$

- Strain energy density:

$$\psi^e = g\psi^e_{\langle A\rangle} + \psi^e_{\langle I\rangle},$$
$$\psi^e_{\langle A\rangle} = \frac{1}{2}\lambda \langle \mathrm{tr}(\boldsymbol{\varepsilon})\rangle_+^2 + G\boldsymbol{\varepsilon}^+ : \boldsymbol{\varepsilon}^+,$$
$$\psi^e_{\langle I\rangle} = \frac{1}{2}\lambda \langle \mathrm{tr}(\boldsymbol{\varepsilon})\rangle_-^2 + G\boldsymbol{\varepsilon}^- : \boldsymbol{\varepsilon}^-,$$

- Fracture energy density:

$$\psi^f = \frac{\mathcal{G}_c}{c_0 l}\left(\alpha + l^2 \boldsymbol{\nabla} d \cdot \boldsymbol{\nabla} d\right),$$
$$\alpha = d^2, \quad g = (1-d)^2.$$

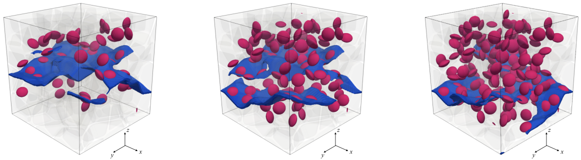

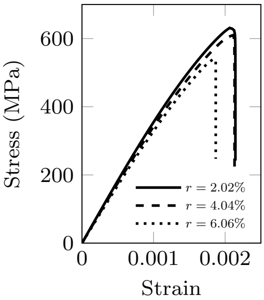

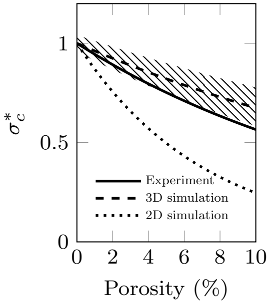

- A set of random close-packing voronoi structures are realized by maximal Poisson-disk sampling.
- The microstructure is generated using a phase-field grain growth model [11].
- Grain boundaries have an arbitrarily high fracture toughness to facilitate intergranular fracture.
- Numerical studies are performed to investigate the effects of bubble geometry, loading conditions, and porosity on the critical fracture strength.
- Results of 15 realizations of 3 porosity levels are fitted using the relation suggested by experiments [12]:

$$\frac{\sigma_c}{\sigma_0} = \exp(-ar).$$

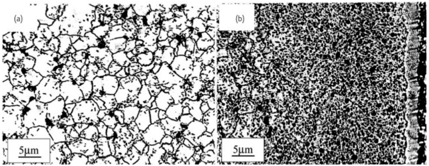

Background:

- Utilities are seeking to increase the allowable burnup limit for UO_2 fuel.
- The risk of fragmentation during a loss-of-coolant accident (LOCA) is a major limitation.
- Over-pressurization of fission gas bubbles results in fine fragmentation of high burnup structures.
- A model for predicting the onset of fragmentation is essential.

External pressure power:

$$\mathcal{P}^{\text{ext}} = -\int_{\Omega_0} \bar{p} \boldsymbol{\nabla} d \cdot \dot{\boldsymbol{\phi}} I_{,d} \, \mathrm{d}V.$$

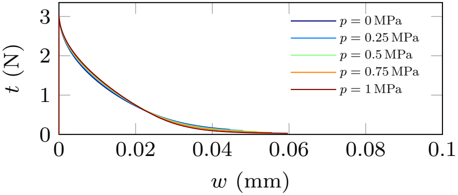

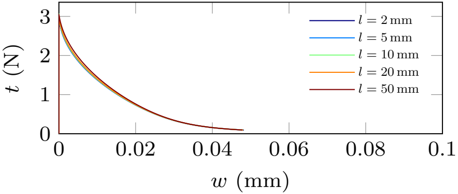

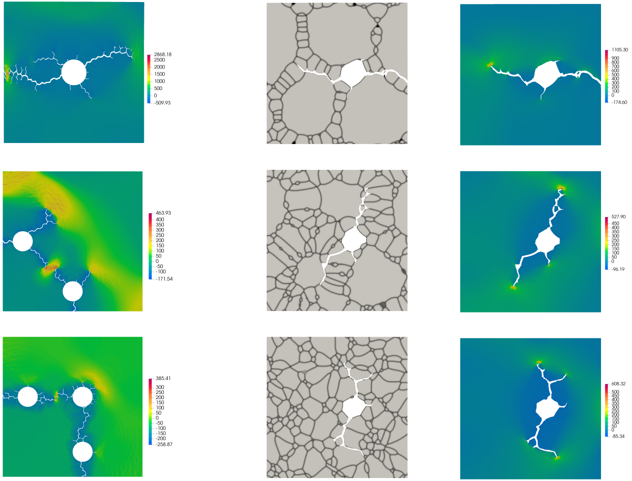

- A 2D REV is considered. Plane strain conditions are assumed to hold.
- LOCA pressure transients:
  - The temperature as a function of time at the edge of a representative pellet for each rod is obtained from simulations.
  - The temperature transient is used as an input to a Kim-Kim-Suzuki (KKS) phase-field model [13] to determine the pressure transient.
  - The pressure transient is treated as a known in the fracture model.
- Effects of bubble size, bubble pressure, surrounding pressure, and multi-bubble interaction are investigated.
- Defect evolution and recrystallization can be incorporated into the fracture model.

Introduction
Background
Phase-field approach to fracture

The Variational Framework
Thermodynamics
The variational statement

Numerical Examples and Applications
Towards Ductile Fracture
Intergranular Fracture in Polycrystalline Materials
Soil Desiccation

Conclusions and Future Work

Acknowledgements

References

Background:

- Film-substrate systems widely exist in nature and in engineering applications.
- Fracture of thin films has been studied using model-based simulations based on a wide range of methodologies.
- Many soil materials are "cohesive" in nature. It calls for a phase-field model for cohesive fracture.
- Many film-substrate systems are symmetric or axisymmetric. It is important to incorporate stochastic models for material properties.

Model:

- Enforcing traction-free boundary conditions:

$$
\begin{aligned}
&\psi^e = g\psi^e_{\langle A\rangle} + \psi^e_{\langle I\rangle},\\
&\psi^e_{\langle A\rangle} = \frac{1}{2}\boldsymbol{\sigma}_{\langle A\rangle} : \boldsymbol{\varepsilon}, \quad \psi^e_{\langle I\rangle} = \frac{1}{2}\boldsymbol{\sigma}_{\langle I\rangle} : \boldsymbol{\varepsilon},\\
&\boldsymbol{\sigma}_{\langle A\rangle} = \boldsymbol{\sigma}^+_n + \boldsymbol{\sigma}_t, \quad \boldsymbol{\sigma}_{\langle I\rangle} = \boldsymbol{\sigma}^-_n,\\
&\boldsymbol{\sigma}^\pm_n = \langle -t_N\rangle_\pm \, \widetilde{\mathbf{n}} \otimes \widetilde{\mathbf{n}}, \quad \boldsymbol{\sigma}_t = \boldsymbol{\sigma} - \boldsymbol{\sigma}^+_n - \boldsymbol{\sigma}^-_n.
\end{aligned}
$$

- Cohesive fracture:

$$
\alpha = \xi d - (1-\xi)d^2, \quad g = \frac{1}{1+\phi},
$$

$$
\phi = \frac{a_1 d + a_1 a_2 d^2 + a_1 a_2 a_3 d^3}{(1-d)^p}.
$$

- A nonlinear softening law:

$$
\xi = 1, \quad p = 2, \quad a_1 = \frac{\mathcal{G}_c}{c_0 l \psi_c}, \quad a_2 = 1, \quad a_3 = 0.
$$

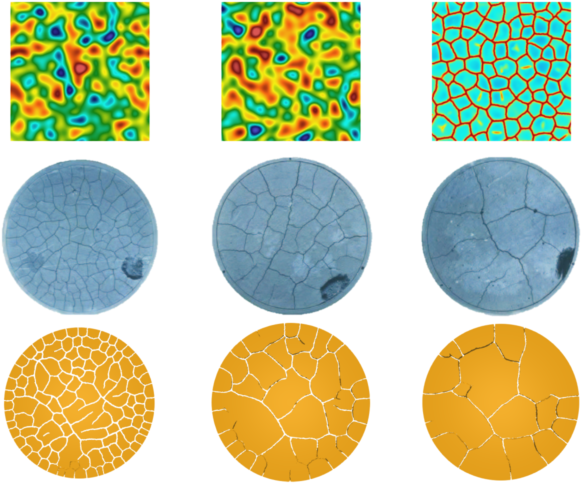

- Only "channeling" cracks in the thin film are considered.
- Thermal effects are neglected. Dehydration is modeled as pre-stress (or equivalent eigenstrains).
- The fracture model is verified with analytical solutions in a periodic quasi-1D context.
- Pervasive fracture is studied with a 2D simplification.
- Material property inhomogeneity is represented by two pointwise correlated random fields $\{\mathcal{G}_c(\boldsymbol{X}), \boldsymbol{X} \in \Omega\}$ and $\{\psi_c(\boldsymbol{X}), \boldsymbol{X} \in \Omega\}$.
- The versatility offered by the probabilistic framework is highlighted by solving a 3D problem based on physical experiments.

Introduction
- Background
- Phase-field approach to fracture

The Variational Framework
- Thermodynamics
- The variational statement

Numerical Examples and Applications
- Towards Ductile Fracture
- Intergranular Fracture in Polycrystalline Materials
- Soil Desiccation

Conclusions and Future Work

Acknowledgements

References

Conclusions:

- A variational framework is proposed to model general dissipative solids with fracture.
- Several models are constructed within the framework to study practical engineering problems:
  - Intergranular fracture: brittle fracture, quasi-brittle fracture, fragmentation, pressurized cracks;
  - Soil desiccation: cohesive fracture, traction-free BCs, random fracture properties;
  - Ductile failure: no re-calibration, regularization-independent response (J-resistance curves), thermal effects, three-point bending, the Sandia Fracture Challenge, oxide spallation in HTHX.

Conclusions:

- A variational framework is proposed to model general dissipative solids with fracture.
- Several models are constructed within the framework to study practical engineering problems:
  - Intergranular fracture: brittle fracture, quasi-brittle fracture, fragmentation, pressurized cracks;
  - Soil desiccation: cohesive fracture, traction-free BCs, random fracture properties;
  - Ductile failure: no re-calibration, regularization-independent response (J-resistance curves), thermal effects, three-point bending, the Sandia Fracture Challenge, oxide spallation in HTHX.

Future work:

- Fracture nucleation with arbitrary strength surface.
- Ductile failure with impact loading, where dynamic effects, abrupt thermal softening, and heat generation are important.
- Fatigue effects are important in structures subject to cyclic loading. Existing fatigue models do not fit into the framework as is. The interplay between fatigue and plasticity could be interesting.

Support from

NEAMS and EPRI for the intergranular fracture projects,
Army Research Office for the soil desiccation project,
Sandia National Labs for the ductile fracture projects,
Idaho National Lab for the oxide spallation project, and
the INL Graduate Fellowship

are greatly appreciated.

I want to thank

Professor John Dolbow for his valuable advice, barbecues and Thanksgiving dinners;
Dr. Benjamin Spencer, Dr. Wen Jiang and everyone in C650 for two great summer internship experiences;
my committee: Professors Wilkins Aquino, Johann Guilleminot, Manolis Veveakis for their time and service, and help with my course projects;
Dr. Brandon Talamini, Dr. Andrew Stershic, and Dr. Michael Tupek for many enlightening discussions;
my colleagues Dr. Yingjie Liu and Dr. Rudy Geelen for babysitting me during my first semesters;
Professor Philip Bayly for his patient guidance in my first research project.

I am most thankful for Peiyi and my puppy Rudy.

[1] Blaise Bourdin, Gilles A Francfort, and Jean-Jacques Marigo.
The variational approach to fracture.
Journal of elasticity, 91(1):5–148, 2008.

[2] Roberto Alessi, Jean-Jacques Marigo, and Stefano Vidoli.
Gradient damage models coupled with plasticity and nucleation of cohesive cracks.
Archive for Rational Mechanics and Analysis, 214(2):575–615, November 2014.

[3] Roberto Alessi, Jean-Jacques Marigo, and Stefano Vidoli.
Gradient damage models coupled with plasticity: Variational formulation and main properties.
Mechanics of Materials, pages 351–367, 2015.

[4] Roberto Alessi, Jean-Jacques Marigo, Corrado Maurini, and Stefano Vidoli.
Coupling damage and plasticity for a phase-field regularisation of brittle, cohesive and ductile fracture: One-dimensional examples.
International Journal of Mechanical Sciences, 149:559–576, December 2018.

[5] M. Ambati, T. Gerasimov, and L. De Lorenzis.
Phase-field modeling of ductile fracture.
Computational Mechanics, 55(5):1017–1040, May 2015.

[6] Marreddy Ambati, Roland Kruse, and Laura De Lorenzis.
A phase-field model for ductile fracture at finite strains and its experimental verification.
Computational Mechanics, 57(1):149–167, 2016.

[7] Christian Miehe, Fadi Aldakheel, and Arun Raina.
Phase field modeling of ductile fracture at finite strains: A variational gradient-extended plasticity-damage theory.
International Journal of Plasticity, 84:1–32, September 2016.

[8] Michael J Borden, Thomas JR Hughes, Chad M Landis, Amin Anvari, and Isaac J Lee.
A phase-field formulation for fracture in ductile materials: Finite deformation balance law derivation, plastic degradation, and stress triaxiality effects.
Computer Methods in Applied Mechanics and Engineering, 312:130–166, 2016.

[9] Michael J. Borden, Thomas J. R. Hughes, Chad M. Landis, Amin Anvari, and Isaac J. Lee.
Phase-field formulation for ductile fracture.
In Advances in Computational Plasticity: A Book in Honour of D. Roger J. Owen, volume 46, page 443. Springer International Publishing, September 2017.

[10] Fei Xue, Tian-Le Cheng, and You-Hai Wen.
Stress analysis of the steam-side oxide of boiler tubes: Contributions from thermal strain, interface roughness, creep, and oxide growth.
Oxidation of Metals, 93(5):515–543, 2020.

[11] N. Moelans, B. Blanpain, and P. Wollants.
Quantitative analysis of grain boundary properties in a generalized phase field model for grain growth in anisotropic systems.
Phys. Rev. B, 78:024113, Jul 2008.

[12] M. Oguma.
Microstructure effects on fracture strength of UO_2 fuel pellets.
Journal of Nuclear Science and Technology, 19(12):1005–1014, 1982.

[13] L. K. Aagesen, S. Biswas, W. Jiang, A. M. Jokisaari, D. Andersson, M. W. D. Cooper, and C. Matthews.
Determine fragmentation criteria in high-burnup UO_2 fuel during accident conditions.
Technical Report INL/EXT-20-00558, Idaho National Laboratory, 2020.